Journal Pre-proofs

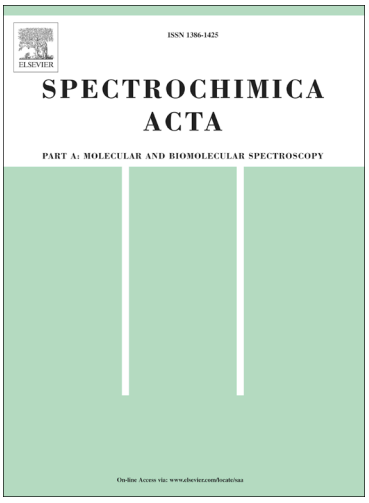

Cyanine-modified near-infrared upconversion nanoprobe for ratiometric sensing of N_2H_4 in living cells

Chuan-Jian Li, Min-An Ye, Pei-Pei Su, Cheng Yao, Yi Zhou

PII: S1386-1425(20)31132-X
DOI: https://doi.org/10.1016/j.saa.2020.119153
Reference: SAA 119153

To appear in: *Spectrochimica Acta Part A: Molecular and Biomolecular Spectroscopy*

Received Date: 2 April 2020
Revised Date: 19 October 2020
Accepted Date: 26 October 2020

Please cite this article as: C-J. Li, M-A. Ye, P-P. Su, C. Yao, Y. Zhou, Cyanine-modified near-infrared upconversion nanoprobe for ratiometric sensing of N_2H_4 in living cells, *Spectrochimica Acta Part A: Molecular and Biomolecular Spectroscopy* (2020), doi: https://doi.org/10.1016/j.saa.2020.119153

Cyanine-modified near-infrared upconversion nanoprobe for ratiometric sensing of N_2H_4 in living cells

Chuan-Jian Li, Min-An Ye, Pei-Pei Su, Cheng Yao, and Yi Zhou*

College of Chemistry and Molecular Engineering, Nanjing Tech University, Nanjing 211816, P. R. China

**Corresponding authors.*

Tel: (+86) 025-5813-9482

Fax: (+86) 025-5813-9482

E-mail: zhouyinjtech@njtech.edu.cn; zhouyinjtech@126.com (Assoc. Prof. Y. Zhou);

Graphical Abstract

The following scheme illustrated the synthesis route of CQM1-UCNPs. Firstly, The cyanine dye (CQM1) was synthesized. Then, OA-UCNPs was modified with α-cyclodextrin (CD). Next, CD-UCNPs was used as a carrier for encapsulating dye (CQM1). When N_2H_4 was added, the UCL intensity of the nanoprobe (CQM1-UCNPs) would change.

Research Highlights

- A cyanine-modified ratiometric upconversion nanoprobe was established for the specific detection of hydrazine.
- A cyanine-based upconversion nanoprobe can quantitatively detect the concentration of hydrazine in solution.
- CQM1-UCNPs exhibited larger ratiomertric luminescent UCL change, high selectivity and low detection limit.
- CQM1-UCNPs showed good biocompability and could reliably detect intracellular hydrazine level changes in living cells with a ratiometric method.

ABSTRACT

Although being as an important chemical material in industry, hydrazine (N_2H_4) is highly toxic to the humans and animals. The development of sensitive methods for the detection of hydrazine is meaningful. Herein, we develop a new organic-inorganic hybrid nanoprobe for the detection of N_2H_4 based on luminescent resonance energy transfer (LRET) process. The nanoprobe contains N_2H_4-responsive NIR cyanine dye (CQM1) and α-cyclodextrin (CD) anchored on the surface of lanthanide-doped upconversion nanophosphors (UCNPs). In the presence of hydrazine, the hybrid materials (CQM1-UCNPs) showed the a large ratiometric luminescent signal change with high sensitivity and selectivity. More importantly, by taking advantage of ratiometric Upconversion luminescent (UCL) signal and the features of NIR emission/excitation, the nanoprobe was successfully applied for visualization of hydrazine in living cells for the first time.

Keywords: Hydrazine, Ratiometric, NIR-excited imaging, Upconversion nanoprobe

1. Introduction

Hydrazine (N_2H_4) is an important class of chemical reagents with basic and reducing properties that plays a vital role in the synthesis of various kinds of catalysts, metal anticorrosion, polymers, textile dyes, pharmaceuticals and so on [1-3]. In particular, hydrazine is widely used as a high-energy propellant in space vehicles due to its flammable and detonable nature [4-5]. In the spite of its broad industrial applications, hydrazine liquids and vapors can easy entrance human body by inhalation and skin absorption, leading to a series of serious health problems including infections of the respiratory tract, central nervous system and organ damage [6-7]. Considering the reported potentially carcinogenic effect of hydrazine on the human health, the total concentration of hydrazine is strictly regulated to be < 10 ppb in the drinking water by the U.S. Environmental

Protection Agency (EPA) [8]. Therefore, the development of convenient and reliable methods for monitoring hydrazine in living systems is highly desirable.

Fluorescence assays has been considered as a powerful strategy to track biologically and environmentally important species due to their several merits such as convenience, relatively low costs, high spatiotemporal resolution and noninvasiveness, excellent compatibility for biological samples [9-13]. Due to the strong nucleophilic characteristic of hydrazine, a variety of reactive organic chromophores for hydrazine detection have been designed with a recognition moiety, such as acetyl [14,15], 4-bromobutyrate [16-19], levulinate [20-22], phthalimide [23-25], β-diketone [26-27], vinyl malononitrile [28-30], and others [31,32]. Although much progress has made in this field, most of the reported hydrazine-sensitive fluorescent probes displayed fluorescent emission under excitation of UV or visible light and suffer from background autofluorescence by biomolecules in the living systems, which limit their practical application.

Based on above-mentioned consideration, rare earth-doped upconversion nanoparticles (UCNPs), which are tunable materials, have been considered a promising candidate to replace traditional downconversion materials. They can efficiently convert near-infrared excitation into shorter wavelength emissions via a two-photon or multiphoton mechanisms [33]. As a result, UCNPs show attractive characteristics for their use in sensing and bioimaging due to the advantages of non-autofluorescence from biological samples, higher light penetration depth, no photo-bleaching, large anti-Stokes shift of several hundred nanometers and chemical stability [34-36].

Recently, various luminescence resonance energy transfer (LRET) based upconversion nanoprobes have been successfully developed for detection or bioimaging of small molecules [37,38], biomacromolecules [39-41] and metal ions [42-46]. However, the responsive upconversion luminescent (UCL) emission of majority of the reported upconversion nanoprobes under the visible range, which further impeded their application in depth bio-detection. To the best of our knowledge, using upconversion luminescent detection method for hydrazine in living cells have not been reported to date.

Herein, we developed a hydrazine-selective near-infrared UCL nanoprobe with NIR-excited ratiometric signals. This assembled nanoprobe took advantage of α-cyclodextrin (CD) with hydrophilic outer surface and lipophilic cavity modified OA-UCNPs ($NaYF_4$:20%Yb, 1.8%Er,

0.5%Tm) as carrier of the N_2H_4-reponsive NIR cyanine dye (CQM1), which could be employed for UCL monitoring of hydrazine in aqueous solution. Furthermore, benefited from the features of NIR emission and NIR excitation of UCNPs and ratiometric UCL signals, the hybrid nanoprobe (CQM1-UCNPs) has been proved to be capable of UCL imaging of intracellular hydrazine.

2. Experimental section

2.1. Instruments and reagents

All reagents and chemicals were purchased from commercial sources and used without further purification. 2,3,3-trimethylindolenine, 10-bromoundecanoic acid, acetyl bromide and triethylamine were obtained from Aladdin. Oleic acid, 1-octadecane and ammonium fluoride were obtained from Sigma-Aldrich. Rare chloride hexahydrate $YCl_3•6H_2O$ (99.9%), $YbCl_3•6H_2O$ (99.9%), $ErCl_3•6H_2O$ (99.9%) and $TmCl_3•6H_2O$ (99.9%) were purchased from Alfa Aesar. Absolute ethanol, cyclohexane, toluene, phosphorus oxychloride, sodium acetate, acetonitrile, n-butanol and methylene chloride were of analytical grade and purchased Sinopharm Chemical Reagent Co, Ltd. Water in the experiment was purified from the Milli-Q system. ^{1}H-NMR and ^{13}C-NMR were measured on a Bruker 400 MHz MNR spectrometer. Electrospray ionization mass spectra (ESI-MS) were measured on a Micromass LCTTM system. Powder X-ray diffraction measurements were performed on a Bruker D8 diffractometer at a scanning rate of 1°/min with the 2θ range from 10 to 90°, with Cu Kα irradiation (λ=1.5406 Å). Transmission electron microscope (TEM) images were observed using a transmission electron microscope (TEM) (Talos L120C, USA). HR-TEM were performed on a JEOL JEM-2100F transmission electron microscope with an accelerating voltage of 200 kV. Uv–vis spectral were obtained using a Perkin Elmer Lambda 35 spectrometer. Upconversion luminescence spectra were recorded on a Perkin Elmer LS50B fluorescence spectrometer equipped with a 980 nm continuous-wave laser (Beijing Hi-Tech Optoelectronic Co., Ltd.) as the excitation source. FTIR spectra were recorded using a Nicolet iS50 FTIR instrument.

2.2. Synthesis and characterization of nanoprobe

Compound 1: Compound 1 was prepared according to a literature method [47]. Phosphorus

oxychloride (37.0 mL, ~400 mmol) in anhydrous DCM (40 mL) was added dropwise to N, N-dimethylformamide (40.0 mL, ~510 mmol) at under an ice bath. After stirring for 30 min, cyclohexanone (10 g, 100 mmol) was added and refluxed for 4 h. The reaction mixture was poured into ice-cold water and kept it overnight to produce a large amount of light yellow precipitate. The product was filtered and washed with water/acetone (9/1, v/v). The crude product was dried in vacuum and can be used directly for next reaction.

Compound HC1: 2, 3, 3-trimethylindolenine (1.59 g, 10.0 mmol) and 11-bromoundecanoic acid (2.65 g, 10.0 mmol) were dissolved in acetonitrile (100 mL) and refluxed with continuous stirring for 24 h. Then, the solvent was removed under reduced pressure and the resulted residue was treated diethyl ether (50 ml) for 24 h at the room temperature. Finally, a powder-red solid was obtained under vacuum filtration and can be used directly for next reaction.

Compound HC2: Synthesized analogously to HC1

Compound CQ1: Compound 1 (105 mg, 0.61 mmol) and compound 2 (560 mg, 1.32 mmol) were dissolved in the mixture solvent of 1- butanol/toluene (v:v = 2:1) and stirred at 120 °C for 12h. After completion, the solvent was evaporated under reduced pressure. The crude product was purified by silica gel column chromatography using gradient CH_2Cl_2 to CH_2Cl_2/0-5% methanol as eluent to give CQ1 as a dark green solid (266mg, 43%). ^{1}H NMR (400 MHz, $CDCl_3$): δ 8.32 (d, J = 14.1 Hz, 2H), 7.38 (t, J = 7.6 Hz, 4H), 7.26 (s, 1H), 7.23 (d, J = 7.6 Hz, 1H), 7.15 (d, J = 7.9 Hz, 2H), 6.22 (d, J = 14.1 Hz, 2H), 4.19 (t, J = 7.2 Hz, 4H), 4.04 (t, J = 6.7 Hz, 4H), 2.72 (t, J = 6.0 Hz, 4H), 2.26 (t, J = 7.5 Hz, 4H), 2.02–1.94 (m, 2H),1.87–1.80 (m, 4H), 1.70 (s, 12H), 1.6–1.54 (m, 8H), 1.48–1.40 (m, 4H), 1.39–1.32 (m, 8H), 1.25 (s, 16H), 0.90 (t, J = 7.4 Hz, 6H). ^{13}C NMR (100 MHz, $CDCl_3$): δ 173.9, 172.3, 150.4, 144.2, 142.2, 141.0, 128.8, 127.1, 125.3, 122.3, 110.9, 101.2, 64.0, 49.3, 44.9, 34.3, 30.6, 29.3, 29.1, 29.0, 28.1, 28.1, 27.4, 27.0, 26.5, 24.9, 20.7, 19.1, 13.7. *ESI*-MS: m/*z* 935.8 $[M\text{-}Br]^+$.

Compound CQ2: Synthesized analogously to CQ1 (455mg, 52%). ^{1}H NMR (400 MHz, $CDCl_3$): δ 8.34 (d, J = 14.1 Hz, 2H), 7.39 (d, J = 7.5 Hz, 4H), 7.28 (d, J = 5.0 Hz, 1H), 7.25 (d, J = 7.7 Hz, 1H), 7.19 (d, J = 7.9 Hz, 2H), 6.27 (d, J = 14.1 Hz, 2H), 4.25 (t, J = 7.2 Hz, 4H), 4.05 (t, J = 6.7 Hz, 4H), 2.75 (s, 4H), 2.34 (t, J = 7.3 Hz, 4H), 2.03–1.96 (m, 2H), 1.88 (dt, J = 15.0, 7.6 Hz, 6H), 1.72 (s, 16H), 1.57 (dd, J = 14.8, 6.8 Hz, 6H), 1.40–1.32 (m, 4H), 0.92 (t, J = 7.4 Hz, 6H). ^{13}C NMR (100 MHz, $CDCl_3$): δ 173.4, 172.3, 150.4, 144.3, 142.1, 141.0, 128.8, 127.3, 125.3,

122.23, 111.0, 101.3, 64.2, 49.3, 49.3, 44.7, 33.9, 30.6, 28.1, 26.6, 26.4, 24.6, 20.7, 19.1, 13.7. ESI-MS: m/z 795.5 $[M-Br]^+$.

Compound CQR1: To a solution of sodium acetate (123 mg, 1.5 mmol) in anhydrous DMF (20 ml), CQ1 (507 mg, 0.5 mmol) was added under nitrogen atmosphere. The mixture was refluxed with continuous stirring at 90 °C for 5 h. Then, the solvent was removed under reduced pressure. The residue was subjected by silica gel chromatography with petroleum ether/ethyl acetate (v:v= 4:1) to give CQR1 as a red viscous liquid (429 mg, 86%). ^{1}H NMR (400 MHz, $CDCl_3$): δ 8.17 (d, J = 13.3 Hz, 2H), 7.22–7.14 (m, 4H), 6.90 (t, J = 7.4 Hz, 2H), 6.67 (d, J = 8.0 Hz, 2H), 5.46 (d, J = 13.3 Hz, 2H), 4.07 (t, J = 6.7 Hz, 4H), 3.65 (t, J = 7.4 Hz, 4H), 2.61 (t, J = 5.4 Hz, 4H), 2.29 (t, J = 7.5 Hz, 4H), 1.87 (s, 2H), 1.71 (d, J = 7.0 Hz, 4H), 1.67 (s, 12H), 1.63–1.58 (m, 8H), 1.38 (q, J = 7.5 Hz, 12H), 1.29 (s, 16H), 0.93 (t, J = 7.4 Hz, 6H). ^{13}C NMR (100 MHz, $CDCl_3$): δ 186.3, 174.0, 162.3, 144.2, 139.7, 132.9, 127.6, 126.4, 121.7, 120.4, 106.7, 92.4, 64.1, 46.5, 42.6, 34.4, 30.7, 29.5, 29.4, 29.4, 29.2, 29.1, 28.8, 27.2, 26.2, 25.8, 25.0, 22.6, 19.2, 13.8. ESI-MS: m/z 918.0 $[M+2H]^+$.

Compound CQR2: Synthesized analogously to CQR1 (334 mg, 78%). ^{1}H NMR (400 MHz, $CDCl_3$): δ 8.17 (d, J = 13.1 Hz, 2H), 7.22–7.14 (m, 4H), 6.91 (t, J = 7.4 Hz, 2H), 6.66 (d, J = 8.0 Hz, 2H), 5.45 (d, J = 13.2 Hz, 2H), 4.07 (t, J = 6.7 Hz, 4H), 3.67 (t, J = 7.2 Hz, 4H), 2.60 (s, 4H), 2.33 (t, J = 7.4 Hz, 4H), 1.87 (s, 2H), 1.72 (d, J = 7.4 Hz, 6H), 1.68 (d, J = 10.7 Hz, 12H), 1.64–1.55 (m, 6H), 1.47–1.41 (m, 4H), 1.39–1.34 (m, 4H), 0.93 (t, J = 7.4 Hz, 6H). ^{13}C NMR (100 MHz, $CDCl_3$): δ 173.5, 162.3, 144.1, 139.6, 133.0, 127.6, 126.5, 121.8, 120.5, 106.7, 92.5, 64.2, 46.6, 42.3, 34.1, 30.7, 29.7, 28.8, 26.7, 26.0, 25.8, 24.8, 22.6, 19.2, 13.7. ESI-MS: m/z 777.6 $[M-H]^+$.

Compound CQM1: Under a nitrogen atmosphere and an ice bath, acetyl bromide (0.37mL, 5.0 mmol) was added dropwise to a solution of CQR (498 mg, 0.5 mmol) and triethylamine (0.695 mL, 5.0 mmol) in anhydrous CH_2Cl_2 (10 mL). After stirring at 0 ℃ for 30 min, the mixture was warmed to room temperature and stirred for 5 h. The reaction process was monitored by TLC. The reaction mixture was concentrated under reduced pressure, which was subjected by silica gel chromatography with CH_2Cl_2/methanol (v:v = 25:1) to afford the desired product as a deep green solid (353 mg, 68%). ^{1}H NMR (400 MHz, $CDCl_3$): δ 7.68 (d, J = 14.0 Hz, 2H), 7.37 (d, J = 7.5 Hz, 4H), 7.23 (t, J = 7.4 Hz, 2H), 7.13 (d, J = 7.9 Hz, 2H), 6.12 (d, J = 14.1 Hz, 2H), 4.11 (t, J = 7.0

Hz, 4H), 4.04 (t, J = 6.7 Hz, 4H), 2.66 (s, 4H), 2.52 (s, 3H), 2.26 (t, J = 7.5 Hz, 4H), 1.98 (s, 2H), 1.83–1.77 (m, 4H), 1.64 (s, 12H), 1.61–1.55 (m, 8H), 1.41 (d, J = 9.1 Hz, 4H), 1.37–1.30 (m, 8H), 1.26 (s, 16H), 0.90 (t, J = 7.4 Hz, 6H). ^{13}C NMR (100 MHz, $CDCl_3$): δ 173.9, 171.5, 167.9, 159.7, 142.1, 140.7, 140.1, 128.8, 125.3, 122.3, 122.0, 110.8, 100.5, 64.0, 49.1, 44.6, 34.3, 30.6, 29.6, 29.2, 29.1, 29.0, 28.2, 27.3, 26.9, 24.9, 24.3, 20.8, 20.7, 19.1, 13.6. ESI-MS: m/z 961.7 $[M\text{-}Br]^+$.

Compound CQM2: Synthesized analogously to CQM1 (270 mg, 60%). ^{1}H NMR (400 MHz, CD_3OD): δ 7.81 – 7.70 (m, 2H), 7.48 (d, J = 7.4 Hz, 2H), 7.39 (t, J = 7.7 Hz, 2H), 7.28 (d, J = 7.9 Hz, 2H), 7.24 (t, J = 7.5 Hz, 2H), 6.18 (d, J = 14.1 Hz, 2H), 4.13 (t, J = 7.2 Hz, 4H), 3.99 (t, J = 6.6 Hz, 4H), 3.28–3.26 (m, 4H), 2.65 (t, J = 5.7 Hz, 4H), 2.53 (s, 3H), 2.30 (t, J = 7.2 Hz, 4H), 2.01–1.89 (m, 2H), 1.84–1.75 (m, 4H), 1.64 (s, 12H), 1.56–1.50 (m, 4H), 1.47–1.40 (m, 4H), 1.35–1.29 (m, 4H), 0.89 (t, J = 7.4 Hz, 6H). ^{13}C NMR (100 MHz, CD_3OD): δ 173.8, 172.1, 168.4, 159.7, 142.2, 141.1, 140.1, 128.6, 125.1, 122.2, 121.6, 110.9, 100.3, 63.9, 49.0, 43.6, 33.4, 30.4, 27.2, 26.7, 25.9, 24.3, 23.9, 20.8,19.6, 18.8, 12.8. ESI-MS: m/z 819.7 $[M\text{-}Br]^+$.

Synthesis of OA-UCNPs: OA-UCNPs were synthesized by a modified literature method [48]. $YCl_3 \cdot 6H_2O$ (0.777 mmol), $YbCl_3 \cdot 6H_2O$ (0.20 mmol), $ErCl_3 \cdot 6H_2O$ (0.018 mmol), and $TmCl_3 \cdot 6H_2O$ (0.005 mmol) were dissolved in 10 mL of methanol by sonication. The transparent solution was injected in a 50 mL flask. After removal of the methanol, 7 mL oleic acid and 15 mL 1-octadecene were added in the flask, and the solution was heated to 160 °C for 30 min and then cooled down to room temperature. Thereafter, a solution of NaOH (2.5 mmol) and NH_4F (4 mmol) in methanol (10 ml) was added the above the mixture and stirred for 30 min. Subsequently, the solution was slowly heated and degassed at 120 °C for 10 min to remove methanol and then heated to 305 °C under Ar protection and maintained for 1.5 h. After the solution was cooled naturally, the nanoparticles were precipitated by the addition of ethanol (20 ml), centrifuged and washed with ethanol/cyclohexane (3/1, v/v) for three times. Finally, the product was preserved in 10 ml cyclohexane for further usage.

Synthesis of CD-UCNPs: CD-UCNPs were synthesized by a modified process following a literature method [49]. The OA-UCNPs (20 mg) and the CD (80 mg) were dispersed in 20 mL ethanol-water (1:1, v/v). The mixture was stirred vigorously under room temperature, resulting in a homogeneous solution. After stirring for 20 h, the solvent was removed by centrifugation (10000 rpm, 10 min), and washed alternately with deionized water and ethanol for three times. The

resulting product could be re-dispersed in deionized water.

Assembly of CQM1/CQM2 to the Surface of CD-UCNPs: The as-prepared CD-UCNPs (20 mg) and organic dye CQM1 (10 mg) were dispersed in the 10 mL chloroform by ultrasonication. The mixture was stirred for 5 h at 25 ℃ to from a homogeneous phase. Hybrid materials (CQM1-UCNPs) could be redispersed in water to form a clear deep blue solution, which was further stored at 4 ℃ for spectrum and imaging investigation. CMQ2-UCNPs were assembled analogously to CQM1-UCNPs.

2.3. Sample preparation and measurements

Nanoprobe (CQM1-UCNPs) was dispersed in deionized water to obtain the stock solution (10 mg/ml). The stock solution (10 mM) of various anions (F^-, I^-, Br^-, I^-, ClO^-, SO_4^{2-}, NO_3^-, Cu^{2+}, Zn^{2+}, Mg^{2+}, Fe^{2+}, Al^{3+}) and biothiols (Cys, Hcy, GSH) were prepared in deionized water. All spectroscopic measurements were performed using 0.03 mg/ml of CQM1-UCNPs in the mixture of acetate buffer (pH 4.5, 10 mM) and DMSO (1/9, V/V) at the room atmosphere.

2.4. Cell culture and cytotoxicity assay

Hela cells (cervical cancer cells) were purchased from KeyGen Biotech (Nanjing, China), and were cultured in Dulbecco's modified Eagle's medium (DMEM) supplemented with 10% FBS (fetal bovine serum), penicillin (100 μg mL^{-1}) and streptomycin (100 μg mL^{-1}) in an atmosphere of 5% CO_2 and 95% air at 37°C. The cytotoxicity of CQM1-UCNPs was evaluated by MTT proliferation assay. The cells were seeded in 96-well plates and cultured in growth medium at 37 °C and 5% CO_2 for 24 h. Different amounts of CQM1-UCNPs (0, 100, 250 and 500 μg mL^{-1}) were added into the previous media. After incubation at 37 °C for 24 h, 5 mg ml^{-1} of MTT reagent was added each well and followed by culture for another 4 h. The absorbance of each well was measured with a microplate reader (SPECTRA SLT; Labinstruments, Salzburg, Austria).

2.5. UCL imaging in living cells

Cells imaging was obtained on the an FV1000IX81 confocal microscope equipped with a 980 nm CW laser. Cells were seeded in 96-well plates and cultured under above same conditions. The cells were divided two groups before cell imaging experiments. One group of cells incubated with 0.1 mg/ml CQM1-UCNPs for 30 min at 37 ℃. Another group of cells incubated with 0.1 mg/ml CQM1-UCNPs for 30 min at 37 ℃ and then treated with 50 μM N_2H_4 for another 30 min. After being washing with PBS for three times, the UCL signals were collected in the range of 500-560 nm for green channel, 600-700 nm for red channel and 788-812 nm for NIR emission.

Result and discussion

3.1. Design principle of CQM1-UCNPs for N_2H_4

The upconverison luminescent hybrid nanoprobe (CQM1-UCNPs) was designed relies on the LRET process, in which CQM1 and UCNPs were served as the energy donors and the energy acceptors, respectively. As previously reported by Hu et al [14], the NIR cyanide dye (CQM1) initially exhibited a prominent absorption band at 798 nm. Upon the addition of N_2H_4, the acetate moiety of CQM1 transformed to the enol form of CQR1 (Scheme S2) and corresponding to the maximum absorption of CQM1 blue shifted to 520 nm. The two absorption bands centered at 520 nm and 788 nm, which perfectly overlapped with the UCL emissions of transient bands of Er^{3+} ($^2H_{11/2} \rightarrow {}^4H_{15/2}$, 514–534 nm; $^4H_{3/2} \rightarrow {}^4H_{15/2}$, 534–560 nm; $^4F_{9/2} \rightarrow {}^4F_{15/2,}$ 635–680 nm) and Tm^{3+} ($^3H_4 \rightarrow {}^3H_6$, 755–845 nm) (Fig. 2A). Therefore, the effective luminescent resonance energy transfer (LRET) occurs from UCNPs to CQM1 by the presence or absence of hydrazine (Scheme 1). It should be noted that a new emission band at around 820 nm was observed, which could be attributed the NIR emission of CQM1 when the under excitation by the UCL emission of UCNPs under the 980 nm laser irradiation [50,51]. Subsequently, α-cyclodextrin (CD) was coated with OA-UCNPs via host-guest interaction to improve their solubility. A long alkyl chain was introduced into CMQ1 and further assembly of CD-UCNPs, which not only created a three water-soluble layer nanostructure, but also was useful for improving the loading capacity of dye on the surface of UCNPs.

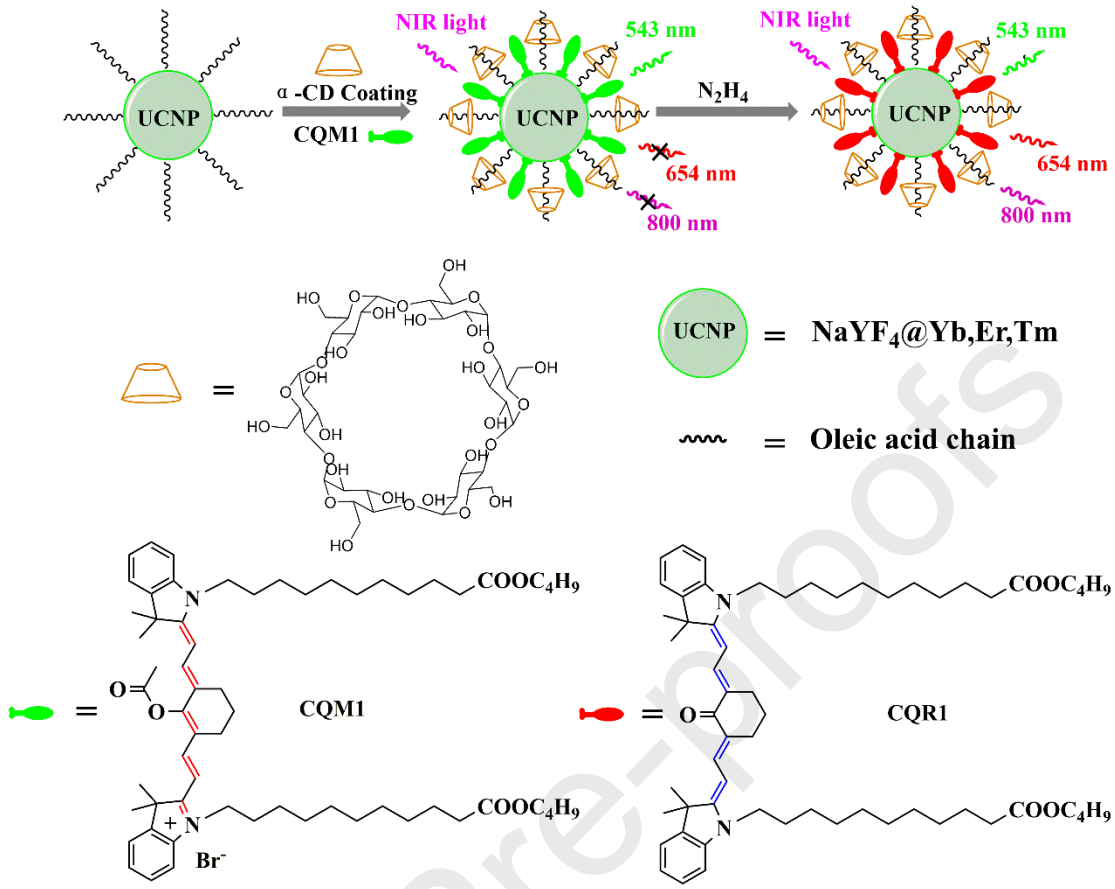

Scheme 1. The structure of CQM1-UCNPs and proposed sensing mechanism with N_2H_4

Synthesis and characteristic of CQM1-UCNPs

The NIR cyanine dye (CQM1) with two long chains of alkyl, which was synthesized through a triethylamine-promoted electrophilic reaction between CQR and acetyl bromide. The Tm^{3+} and Er^{3+}-codopped upconvesion nanoparticles ($NaYF_4$: Yb, Tm, Er) were prepared by a modified solvothermal procedure, and further was modified with α-cyclodextrin (CD). Subsequently, the fabrication of hybrid nanoprobe (CQM1-UCNPs) through a polymer-assisted method based on hydrophobic and hydrophobic reaction [52]. Transmission Electron Microscopy (TEM) images showed that OA-UCNPs and CQM1-UCNPs were highly uniform with an average diameter of ~ 30 nm (Fig. 1A), indicating no significant change in morphology and size of UCNPs after modification of CQM1 dye (Fig. 1B). Fig. 1C showed the power X-ray diffraction (XRD) peaks of CQM1-UCNPs match well with the standard cards of β-$NaYF_4$ (JCPDS NO.16-0034). Moreover, the High-Resolution Transmission Electron Microscopy (HR-TEM) images showed that lattice

fringes with a spacing of 0.516 nm was consistent with the (100) plane of the hexagonal $NaYF_4$ structure (Fig. 1D).

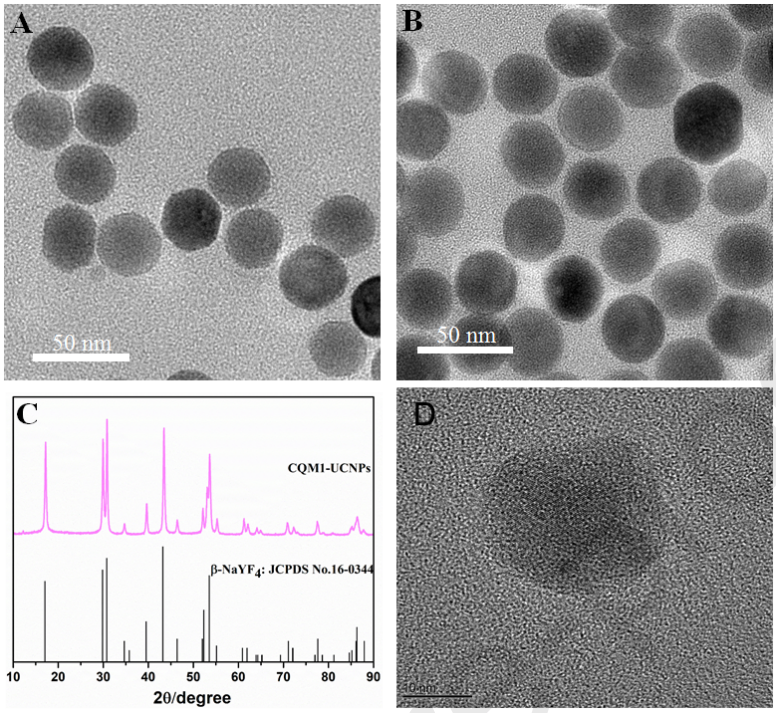

Fig.1. TEM image (A) of OA-UCNPs; TEM (B) and HR-TEM (D) image of CQM1-UCNPs. (C) XRD patterns of CQM1-UCNPs and the standard pattern of pure hexagonal $NaYF_4$ (JCPDS card No.16–0334).

To further confirm assembly of CD and organic dye CMQ1 on the surface of UCNPs, the structures of OA-UCNPs, CD-UCNPs, CQM1, and CQM1-UCNPs were characterized by Fourier-transform infrared (FT-IR) spectroscopy. As shown in Fig. S1, the two peaks at 3443 and 1636 cm^{-1} in the spectra of OA-UCNPs were attributed to δ (O−H) and δ (C=O) in the carboxyl group of OA, and the another two peaks at 2925 and 2853 cm^{-1} were ascribed to C-H stretching (asymmetric and symmetric stretching) of the long alkyl chain. For the FTIR spectrum of CD-UCNPs, a strong peak at 1077 cm^{-1} was attributed to δ (C-O-C) of CD, indicating the presence of CD on the surface of UCNPs. Moreover, the multi-peak bands at 1572, 1433, 1264 cm^{-1} were attributed to δ (=C-H) of the phenyl group in the spectrum of CQM1. All the characteristic features appeared in the spectrum of CMQ1-UCNPs, demonstrating that the successfully assembled of CD and CMQ1 to the surface of OA-UCNPs. Based on the standard-absorption spectra, the loading amount of CMQ1 on the surface of UCNPs was calculated to be ~12.05 wt% (0.03 mg/mL, ~3.76 μM, Fig. S2). Similar to this way, the loading

capacity of short-chained CMQ2 was determined to be ~7.47 wt% (0.03 mg/mL, ~2.33 μM, Fig.S3), which is lower than that of CMQ1, indicating the introduction of long alkyl chain into CMQ1 was of great importance to improving the loading capacity of dye on the surface of UCNPs for sensing of CO concentration in a wide range.

3.3. Spectroscopic response of CQM1-UCNPs toward N_2H_4

The sensing properties of CQM1-UCNPs to N_2H_4 was assessed by UV-vis and UCL spectroscopy. As shown in Fig. 2B, the absorption brand located at 788 nm of CQM1-UCNPs gradually decreased with addition of N_2H_4, and corresponding to increasing of a new absorption band located at 520 nm. In this process, the color of the solution showed a significant change from green to red, indicating CQM1-UCNPs can be used as a colorimetric probe for sensing N_2H_4. The resulting absorbance spectra was consistent with that of CQR1 (Fig. S4). This change in absorption can induce the degree of overlap between the absorption band of CQM1 and UCL emission of UCNPs. According to the Fig. 2D, upon the addition of N_2H_4, the NIR UCL emission at 800 nm and the red UCL emission at 657 nm gradually increased, whereas a significant quenching in the green UCL emission at 543 nm. These results indicated that LRET mechanism could occur between the UCNPs and CQM1. Compared with the UCL intensity of OA-UCNPs, a significant quenching was observed in the NIR emission after assembling of CQM1 to the surface of OA-UCNPs. The quenching LRET efficiency of the NIR UCL emission at 800 nm of CQM1-UCNPs was measured to be ~88.2%. The ratio of the UCL emission intensity at 543 to 657 nm ($UCL_{543\ nm}/UCL_{657\ nm}$) was employed as a ratiometric UCL signal for monitoring the concentration of N_2H_4, which exhibited a decrease linear in the range of 0-132 μM. The detection limitation (DL) of CQM1-UCNPs for N_2H_4 was measured to be ~0.21 μM by using the ratio UCL signals, which lower than that of intensity-based signal detection ($DL_{543\ nm}$: 1.69 μM, $DL_{657\ nm}$: 2.17 μM, $DL_{800\ nm}$: 1.31 μM). Moreover, the ratio UCL signal of detection limit of CQM1-UCNPs is much lower than the reported N_2H_4 fluorescent probes, indicating that CQM1-UCNPs have high sensitivity for the detection of N_2H_4 (Table S1). More importantly, the turn-on NIR UCL emission (800 nm) response of CQM1-UCNPs under the NIR excitation (980 nm), which was beneficial for biological application due to its low auto-fluorescence background and remarkable tissue penetration depth. The time-dependent the UCL emission change was measured of CQM1-UCNPs showed the green UCL emission at 543 nm reached equilibrium with the treatment of N_2H_4 for 15

min (Fig. S9), indicating CQM1-UCNPs could rapidly response to N_2H_4.

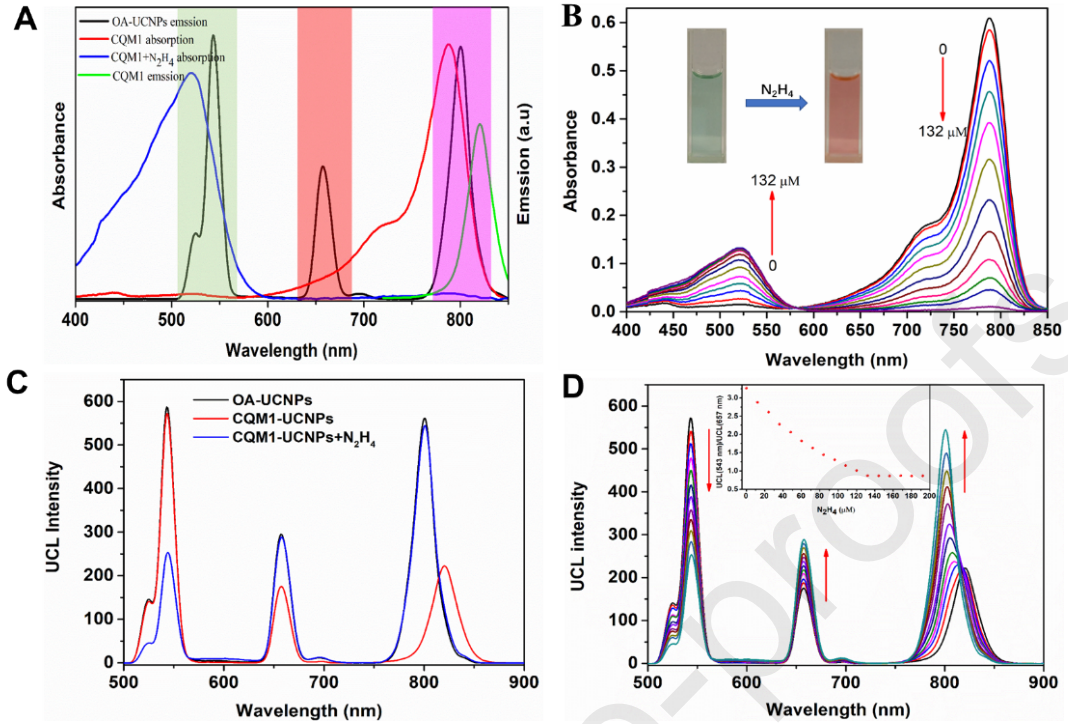

Fig.2. (A) UV–Vis spectra of CQM1 in the absence (red line) and presence of N_2H_4 (blue line); UCL spectra of OA-UCNPs (black line) under 980 nm excitation; The emission spectrum of CQM1 (green line) (B) Absorption spectrum of 0.03 mg/mL of CQM1-UCNPs in the presence of different concentrations of N_2H_4 (0-192 μM) in a mixture of acetate buffer (pH 4.5, 10 mM) and DMSO (1/9, v/v). Inset: the photo shows the color change from green to red. (C) UCL emission spectra of OA-UCNPs, CQM1-UCNPs, and CQM1-UCNPs with the treatment of N_2H_4. (D) UCL spectrum change of 0.03 mg/mL of CQM1-UCNPs upon addition of N_2H_4 (0-192 μM) in a mixture of acetate buffer (pH 4.5, 10 mM) and DMSO (1/9, v/v). Inset: the UCL emission ratio intensity at 543 and 657 nm ($UCL_{543\ nm}/UCL_{657\ nm}$) as a function of N_2H_4 concentration.

The specificity of CQM1-UCNPs toward N_2H_4 was evaluated by measuring the ratio UCL responses to a series of potential interferences including anions (F^-, I^-, Br^-, I^-, ClO^-, SO_4^{2-}, NO_3^-), metal cations (Cu^{2+}, Zn^{2+}, Mg^{2+}, Fe^{2+}, Al^{3+}) and biothiols (Cys, Hcy, GSH). As shown in Fig 3. Only N_2H_4 could lead to a significant decrease in the luminescent intensity ratio ($UCL_{543\ nm}/UCL_{657\ nm}$), and other analytes trigger less effect on the ratiometric signals. These results that indicated CMQ1-UCNPs possessed high sensitivity for N_2H_4 detection.

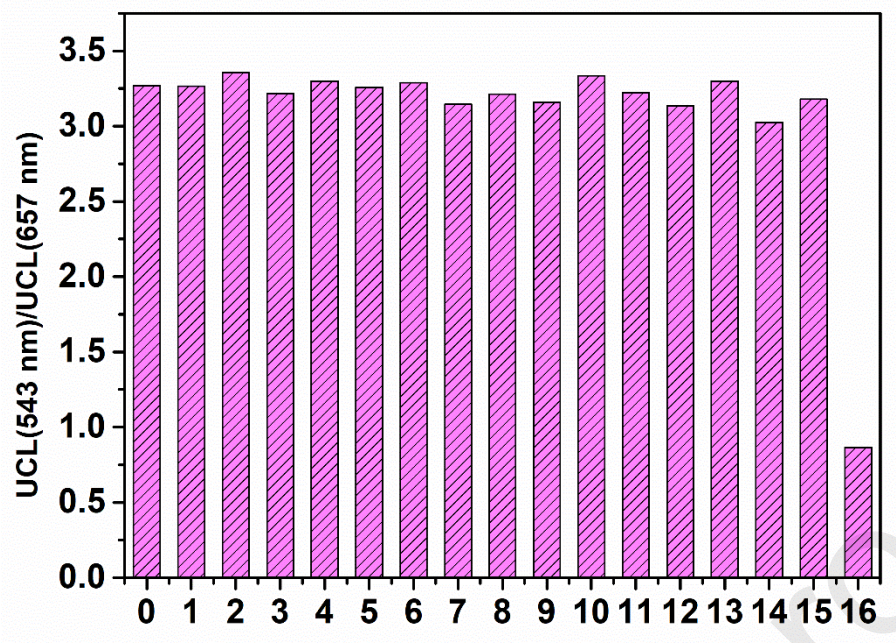

Fig.3. Ratiometric UCL responses of 0.03 mg/mL CQM1-UCNPs with N_2H_4 (150 μM) and other analytes (150 μM): 0 black, 1 F^-, 2 I^-, 3 Br^-,4 Cl^-, 5 ClO^-, 6 SO_4^{2-}, 7 NO_3^-, 8 Cu^{2+}, 9 Zn^{2+}, 10 Mg^{2+}, 11 Fe^{2+}, 12 Al^{3+}, 13 Cys, 14 Hcy, 15 GSH, 16 N_2H_4

3.2. Detection of N_2H_4 in living cells

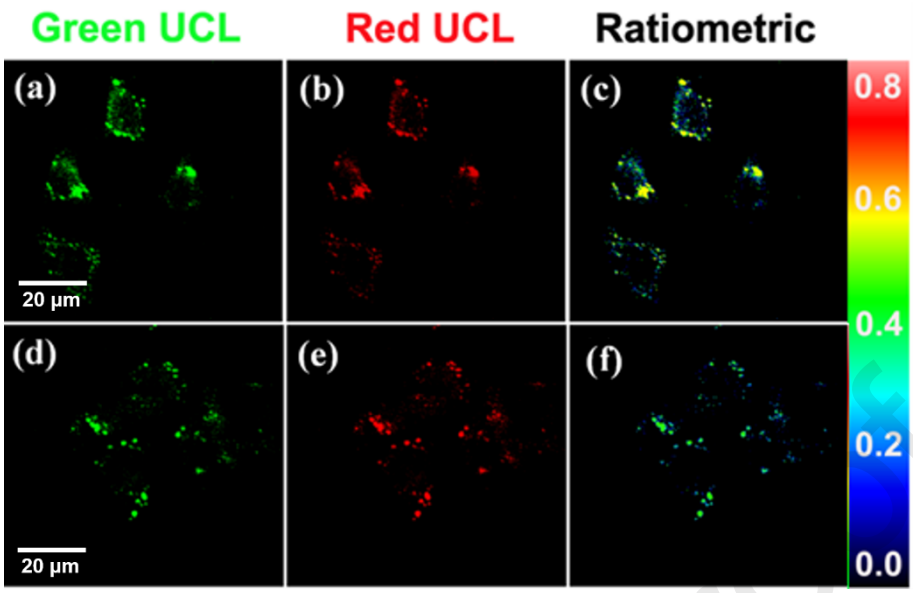

Fig. 4 Ratiometric UCL images in the Hela cells (top row, a-c) and 100 μM N_2H_4-pretreated Hela cells (bottom row, d-f) incubated with CQM1-UCNPs (200 μg/mL) for 30 minutes at 37℃. Emission was collected by both the green channel at 500-560 nm (a and d) and red channel at 600-700 nm (b and e) with excitation at 980 nm. (c and f) Ratiometric UCL images with the ratio of green to red channels.

Encouraged by the high sensitivity and selectivity of CQM1-UCNPs, we attempted to investigate whether CQM1-UCNPs could be used as a useful sensing platform for bioimaging or biosensing. Firstly, the cytotoxicity of CQM1-UNCPs was evaluated by mean of MTT assay (Fig. S10). The results displayed that the cell viability was more than 75% even the concentration of CQM1-UCNPs was up to 1 mg/mL, indicating the minimal cytotoxicity and biocompatibility of CQM1-UCNPs. Based on the results, we further evaluate the potential application of CMQ1-UCNPs for visualization of N_2H_4 in living cells. After the Hela cells incubated with 200 μg/mL CMQ1-UCNPs for 30 min at 37 ℃, a weak UCL emission in the red channel and a strong UCL emission in the green channel were observed under 980 nm excitations. However, when the Hela cells incubated with 200 μg/mL CMQ1-UCNPs for 30 min and then treated with 100 μM N_2H_4, the increased UCL intensity in red emission and the decreased UCL intensity in the green emission were found in the intracellular area. Moreover, we conducted the ratiometric UCL imaging for N_2H_4 with the UCL ratio of the green channel to red channel (Fig. 4). Hela cells incubated with CMQ1-UCNPs for 30 min at 37℃ showed the UCL ratio of green to red emission more than 0.6. However, when pretreated Hela cells with CMQ1-UCNPs were continuously incubated with N_2H_4, the corresponding UCL ratio was decreasing to 0.3. These results

demonstrated that CMQ1-UCNPs possessed good biocampability and could be used for ratiometric UCL monitoring of intracellular N_2H_4.

4. Conclusion

In summary, we developed a highly selective and sensitive nanoprobe for sensing of N_2H_4 based on the CQM1-assembled upconversion nanophosphers. The strong luminescent resonance energy transfer (LRET) taking place between UCNPs and CQM1 after the treatment with N_2H_4, which make CMQ1-UCNPs used as a suitable candidate for ratiometric detection of N_2H_4 with a lower detection limit of 0.21 μM. Moreover, with aid of CQM1-UCNPs, the ratiometric imaging of N_2H_4 in living cells with the features of NIR emission and NIR excitation was realized. Therefore, we believe that the superior characteristics of CQM1-UCNPs could be a promising practical tool for tracking N_2H_4 in the biological systems.

Appendix A. Supplementary data

Supplementary data related to this article can be found at http://dx.doi.org/10.1016/j.dyepig.*****.

Acknowledgment

This work is supported by the Natural Science Foundation of Jiangsu Province (BK20170996), the Natural Science Key Fund for Colleges and Universities of Jiangsu Province (15KJB530006), the Open Fund of the State Key Laboratory of Coordination Chemistry, and the Postgraduate Research and Practice Innovation Program of Jiangsu Province (KYCX19_0863).

References

[1] Narayanan SS, Scholz F. A comparative study of the electrocatalytic activities of some metal

hexacyanoferrates for the oxidation of hydrazine. Electroanal 1999; 11: 465-9.

[2] Khaled KF. Experimental and theoretical study for corrosion inhibition of mild steel in hydrochloric acid solution by some new hydrazine carbodithioic acid derivatives. Appl Surf Sci 2006; 252: 4120-8.

[3] Ragnarsson U. Synthetic methodology for alkyl substituted hydrazines. Chem Soc Rev 2001; 30: 205-13.

[4] Sutton AD, Burrell AK, Dixon DA, Garner EB, Gordon JC, Nakagawa T, Ott KC, Robinson P, Vasiliu M. Regeneration of ammonia borane spent fuel by direct reaction with hydrazine and liquid ammonia. Science 2011; 33: 1426-9.

[5] Zelnick SD, Mattie DR, Stepaniak PC. Occupational exposure to hydrazines: treatment of acute central nervous system toxicity. Aviat Space Envir MD 2003; 74: 1285-91.

[6] Reilly CA, Aust SD. Peroxidase substrates stimulate the oxidation of hydralazine to metabolites which cause single-strand breaks in DNA. Chem Res Toxicol 1997; 10: 328-334.

[7] Garrod S, Bollard ME, Nicholls AW, Connor SC, Connelly J, Nicholson JK, Holmes E. Integrated metabonomic analysis of the multiorgan effects of hydrazine toxicity in the rat. Chem Res Toxicol 2005; 18: 115-122.

[8] Umar A, Rahman MM, Kim SH, Hahn Y-B. Zinc oxide nanonail based chemical sensor for hydrazine detection. Chem Commun 2008; 2: 166-8.

[9] De Silva AP, Gunaratne HQN, Gunnlaugsson T, Huxley AJM, McCoy CP, Rademacher JT, Rice TE. Signaling recognition events with fluorescent sensors and switches. Chem Rev 1997; 97: 1515-66.

[10] Cheng D, Pan Y, Wang L, Zeng Z, Yuan L, Zhang X, Chang Y-T. Selective visualization of the endogenous peroxynitrite in an inflamed mouse model by a mitochondria-targetable two-photon ratiometric fluorescent probe. J Am Chem Soc 2016; 139: 285-92.

[11] Sun M, Guo J, Yang Q, Xiao N, Li Y. A new fluorescent and colorimetric sensor for hydrazine and its application in biological systems. J Mater Chem B 2014; 2: 1846-51.

[12] Cui J, Gao G, Zhao H, Liu Y, Nie H, Zhang X. A highly sensitive and selective fluorescent probe for N_2H_4 in air and living cells. New J Chem 2017; 41: 11891-7.

[13] Chen X, Tian X, Shin I, Yoon J. Fluorescent and luminescent probes for detection of reactive oxygen and nitrogen species. Chem Soc Rev 2011; 40: 4783-804.

[14] Hu C, Sun W, Cao J, Gao P, Wang J, Fan J, Song F, Sun S, Peng X. A ratiometric near-infrared fluorescent probe for hydrazine and its in vivo applications. Org Lett 2013; 15: 4022-5.

[15] Shi X, Huo F, Chao J, Yin C. A ratiometric fluorescent probe for hydrazine based on novel cyclization mechanism and its application in living cells. Sens Actuators, B 2018; 260: 609-16.

[16] Lu Z, Fan W, Shi X, Lu Y, Fan C. Two distinctly separated emission colorimetric NIR fluorescent probe for fast hydrazine detection in living cells and mice upon independent excitations. Anal Chem 2017; 89: 9918-25.

[17] Goswami S, Das S, Aich K, Pakhira B, Panja S, Mukherjee SK, Sarkart S. A chemodosimeter for the ratiometric detection of hydrazine based on return of ESIPT and its application in live-cell imaging. Org Lett 2013, 15: 5412-5.

[18] Qian Y, Lin J, Han L, Lin L, Zhu H. A resorufin-based colorimetric and fluorescent probe for live-cell monitoring of hydrazine. Biosens Bioelectron 2014; 58: 282-6.

[19] Goswami S, Aich K, Das S, Roy SB, Pakhira B, Sarkar, S. A reaction based colorimetric as well as fluorescence 'turn on'probe for the rapid detection of hydrazine. Rsc Adv 2014; 4: 14210-4.

[20] Choi MG, Hwang J, Moon JO, Sung J, Chang S-K. Hydrazine-selective chromogenic and fluorogenic probe based on levulinated coumarin. Org Lett 2011; 13: 5260-3.

[21] Zhu S, Lin W, Yuan L. Development of a near-infrared fluorescent probe for monitoring hydrazine in serum and living cells. Anal Methods 2013; 5: 3450-3.

[22] Yu S, Wang S, Yu H, Feng Y, Zhang S, Zhu M, Yin H, Meng X. A ratiometric two-photon fluorescent probe for hydrazine and its applications. Sens Actuators, B 2015; 220: 1338-45.

[23] Raju MVR, Prakash EC, Chang H-C, Lin H-C. A facile ratiometric fluorescent chemodosimeter for hydrazine based on Ing–Manske hydrazinolysis and its applications in living cells. Dyes Pigments 2014; 103: 9-20.

[24] Cui L, Peng Z, Ji C, Huang J, Huang D, Ma J, Zhang S, Qian X, Xu Y. Hydrazine detection in the gas state and aqueous solution based on the Gabriel mechanism and its imaging in living cells. Chem Commun 2014; 50: 1485-7.

[25] Ali F, Anila H A, Taye N, Mogare DG, Chattopadhyay S, Das A. Specific receptor for hydrazine: mapping the in situ release of hydrazine in live cells and in an in vitro enzymatic assay. Chem Commun 2016; 52: 6166-9.

[26] Lee MH, Yoon B, Kim JS, Sessler JL. Naphthalimide trifluoroacetyl acetonate: a hydrazine-selective chemodosimetric sensor. Chem Sci 2013; 4: 4121-6.

[27] Goswami S, Das S, Aich K, Sarkar D, Mondal TK. A coumarin based chemodosimetric probe for

ratiometric detection of hydrazine. Tetrahedron Lett 2014; 55: 2695-9.

[28] Fan J, Sun W, Hu M, Cao J, Cheng G, Dong H, Song K, Liu Y, Sun S, Peng X. An ICT-based ratiometric probe for hydrazine and its application in live cells. Chem Commun 2012; 48: 8117-9.

[29] Reja SI, Gupta N, Bhalla V, Kaur D, Arora S, Kumar M. A charge transfer based ratiometric fluorescent probe for detection of hydrazine in aqueous medium and living cells. Sens Actuators, B 2016; 222: 923-9.

[30] Zhang R, Zhang C-J, Song Z, Liang J, Kwok RTK, Tang B, Liu B. AIEgens for real-time naked-eye sensing of hydrazine in solution and on a paper substrate: structure-dependent signal output and selectivity. J Mater Chem C 2016; 4: 2834-42.

[31] Zhou D, Wang Y, Jia J, Yu W, Qu B, Li X, Sun X. H-bonding and charging mediated aggregation and emission for fluorescence turn-on detection of hydrazine hydrate. Chem Commun 2015; 51: 10656-9.

[32] Liu L, Le Y, Teng M, Zhou Z, Zhang D, Zhao C, Cao J. A novel fluorescence sensor for hydrazine based on pyrazole formation reaction. Dyes Pigments 2018; 151: 1-6.

[33] Idris NM, Gnanasammandhan MK, Zhang J, Ho PC, Mahendran R, Zhang Y. In vivo photodynamic therapy using upconversion nanoparticles as remote-controlled nanotransducers. Nat Med 2012; 18: 1580-5.

[34] Gorris HH, Wolfbeis OS. Photon-Upconverting nanoparticles for optical encoding and multiplexing of cells, biomolecules, and microspheres. Angew Chem Int Ed 2013; 52: 3584-600.

[35] Zhou J, Liu Q, Feng W, Sun Y, Li F. Upconversion luminescent materials: advances and applications. Chem Rev 2014; 115: 395-465.

[36] Gu B, Zhang Q. Recent Advances on Functionalized Upconversion Nanoparticles for Detection of Small Molecules and Ions in Biosystems. Adv Sci 2018, 5, .1-16.

[37] Mader HS, Wolfbeis OS. Optical ammonia sensor based on upconverting luminescent nanoparticles. Anal Chem 2010; 82: 5002-4.

[38] Zhou Y, Pei W, Zhang X, Chen W, Wu J, Yao C, Huang L, Zhang H, Huang W, Loo JSC, Zhang Q. A cyanine-modified upconversion nanoprobe for NIR-excited imaging of endogenous hydrogen peroxide signaling in vivo. Biomaterials 2015; 54: 34-43.

[39] Deng R, Xie X, Vendrell M, Chang, Y-T, Liu X. Intracellular glutathione detection using MnO2-nanosheet-modified upconversion nanoparticles. J Am Chem Soc 2011; 133: 20168-171.

[40] Cen Y, Wu Y-M, Kong X-J, Wu S, Yu R-Q, Chu X. Phospholipid-modified upconversion nanoprobe for ratiometric fluorescence detection and imaging of phospholipase d in cell lysate and in living cells. Anal chem 2014; 86: 7119-27.

[41] Zhou, Y; Pei WB; Wang CY; Zhu JX; Wu, JS; Yan, QY; Huang, L; Huang, W; Yao, C; Loo, JSC; Zhang, QC. Reactive Oxygen Species: Rhodamine-Modified Upconversion Nanophosphors for Ratiometric Detection of Hypochlorous Acid in Aqueous Solution and Living Cells [J]. Small, 2014, 10, 3560-7.

[42] Liu J, Liu Y, Liu Q, Li C, Sun L, Li F. Iridium (III) complex-coated nanosystem for ratiometric upconversion luminescence bioimaging of cyanide anions. J Am Chem Soc 2011; 133: 15276-9.

[43] Ding Y, Zhu H, Zhang X, Zhu J-J, Burda C. Rhodamine B derivative-functionalized upconversion nanoparticles for FRET-based Fe3+-sensing. Chem Commun 2013; 49: 7797-9.

[44] Liu Y, Jiang A, Jia Q, Zhai X, Liu L, Ma L, Zhou J. Rationally designed upconversion nanoprobe for simultaneous highly sensitive ratiometric detection of fluoride ions and fluorosis theranostics. Chem Sci 2018; 9: 5242-51.

[45] Shi Y, Liu Q, Yuan W, Xue M, Feng W, Li F. Dye-Assembled Upconversion Nanocomposite for Luminescence Ratiometric in Vivo Bioimaging of Copper Ions. ACS Appl Mater Inter 2018; 11: 430-6.

[46] Li Z, Lv S, Wang Y, Chen S, Liu Z. Construction of LRET-based nanoprobe using upconversion nanoparticles with confined emitters and bared surface as luminophore. J Am Chem Soc 2015; 137: 3421-7.

[47] Reynolds GA, Drexhage KH. Stable heptamethine pyrylium dyes that absorb in the infrared. J Org Chem 1977; 42: 885-8.

[48] Li Z, Zhang Y, Jiang S. Multicolor core/shell-structured upconversion fluorescent nanoparticles. Adv Mater 2008; 20: 4765-9.

[49] Wang Y, Wong JF, Teng X, Lin XZ, Yang H. “Pulling” nanoparticles into water: phase transfer of oleic acid stabilized monodisperse nanoparticles into aqueous solutions of α-cyclodextrin. Nano Lett 2003; 3: 1555-9.

[50] Liu J, Liu Y, Bu W, Bu J, Sun Y, Du J, Shi J. Ultrasensitive nanosensors based on upconversion nanoparticles for selective hypoxia imaging in vivo upon near-infrared excitation. J Am Chem Soc 2014; 136: 9701-9.

[51] Guan Y, Qu S, Li B, Zhang L, Ma H, Zhang L. Ratiometric fluorescent nanosensors for selective detecting cysteine with upconversion luminescence. Biosens Bioelectron 2016; 77: 124-30.

[52] Zhou Y, Chen W, Zhu J, Pei W, Wang C, Huang L, Yao C, Yan Q, Huang W, Loo JSC, Zhang Q. Inorganic–Organic Hybrid Nanoprobe for NIR-Excited Imaging of Hydrogen Sulfide in Cell Cultures and Inflammation in a Mouse Model. Small 2014; 10: 4874-85.